Layered α-Co(OH)$_2$ Nanocones as Electrode Materials for Pseudocapacitors: Understanding the Effect of Interlayer Space on Electrochemical Activity

*Lei Wang, Zhi Hui Dong, Zheng Gong Wang, Feng Xing Zhang, and Jian Jin**

The effect of space accessible to electrolyte ions on the electrochemical activity is studied for a system of transition-metal hydroxide-based pseudocapacitors. Layered α-Co(OH)$_2$ with various intercalated anions is used as a model material. Three types of layered α-Co(OH)$_2$ with intercalated anions of dodecyl sulfate, benzoate, or nitrate, are prepared by a simple reflux and an anion-exchange process. Scanning electron microscopy (SEM) and transmission electron microscopy (TEM) observations and X-ray diffraction (XRD) data show the formation of layered α-Co(OH)$_2$ nanocones with interlayer spacing between adjacent Co(OH)$_2$ single sheets of 1.6, 0.7, and 0.09 nm, corresponding to the anions as listed above. Electrochemical characterization reveals that interlayer space has a great effect on the electrochemical activity of α-Co(OH)$_2$ nanocones as an electrode material. For the interlayer spacing of 1.6 nm, in the case of dodecyl sulfate-intercalated α-Co(OH)$_2$, the Faradaic reaction takes place more adequately than for benzoate- and nitrate-intercalated α-Co(OH)$_2$. As a result, a higher specific capacitance and better cycling stability is obtained for the dodecyl sulfate-intercalated α-Co(OH)$_2$. The electrochemical activity obviously reduces when the interlayer space decreases to 0.7 nm. Our results suggest the importance of rational designing the interlayer space of layered transition metal hydroxides for high-performance pseudocapacitors.

1. Introduction

The ever-worsening global warming and energy scarcity issues call for not only urgent development of clean alternative energies and emission control of greenhouse gases, but also more advanced energy storage and management systems. Electrochemical capacitors (ECs), also called pseudocapacitors or supercapacitors (SCs), which are energy storage devices that use Faradaic reactions or ion adsorption on the surface of active materials to store charge, have numerous advantages over other power-source technologies.[1–4] From a materials point of view, there are three main categories of ECs: i) carbon-based electric double-layer capacitors (EDLCs), which exploit the electrostatic separation between electrolyte ions and high-surface area electrodes; ii) electronically conducting polymers, which store energy through fast reversible doping and de-doping processes; and, iii) pseudocapacitive transition-metal-based oxides or hydroxides, which store energy on the basis of fast reversible multi-electron surface redox Faradaic reactions. In order to improve the capacity of ECs, numerous efforts have been made to investigate pseudocapacitive transition-metal-based oxides or hydroxides, such as MnO_2,[5–10] NiO_x,[11,12] CoO_x,[13–18] $Co(OH)_2$,[19–23] and $Ni(OH)_2$,[24–27] because they can produce much higher specific capacitances than typical carbon-based EDLCs and electronically conducting polymers.

It has been widely accepted that only surface atoms or a very thin layer of active electrode materials play a key role during pseudocapacitive process.[28,29] From this point of view, electrochemical activities and the microstructures of active electrode materials are closely related. Considerable attention over the past decade has been paid to designing and developing advanced materials with dimensions in the nanometer scale. Nanostructured electrode materials usually lead to better electrochemical performance than traditional materials because the distances across which the electrolytes need to transport ions within nanostructured electrode materials is dramatically smaller than those for bulk materials. Moreover, the hollow spaces (or holes) in the active materials are also beneficial to electrochemical activity. Therefore, increasing the specific surface area of the active electrode materials for maximized access of electrolyte is undoubtedly a significant means to achieve high-performance pseudocapacitors.[30,31] However, the long-held view has been that hollow spaces smaller than the size of solvated electrolyte ions are incapable of contributing to charge storage. This lower size limit of accessible hollow space must be considered when designing nanostructured electrode materials with rational microstructures. The effect of the pore-size limit on capacitance was studied in the system of conductive

L. Wang, Z. H. Dong, Z. G. Wang, Prof. J. Jin
i-LAB and Nano-Bionics Division
Suzhou Institute of Nano-Tech and Nano-Bionics
Chinese Academy of Sciences
Suzhou, Jiangsu 215123, P. R. China
E-mail: jjin2009@sinano.ac.cn
L. Wang, Prof. F. X. Zhang
Key Laboratory of Synthesis and Natural Functional Molecular Chemistry (Ministry of Education)
College of Chemistry & Materials Science
Northwest University,
Xi'an, Shaanxi 710069, P. R. China

DOI: 10.1002/adfm.201202786

porous carbon by Gogotsi et al.[32] and an anomalous increase in carbon capacitance at pore sizes less than 1 nm was verified; however, until now, no such studies had addressed pseudocapacitive electrode materials, such as transition metal oxides or hydroxides.

In this article, we use layered α-$Co(OH)_2$ with tunable interlayer space as a model material to investigate the effect of hollow space on capacitance. Layered α-$Co(OH)_2$ is a class of lamellar compounds that consists of positively charged brucite-like cobalt host layers and hydrated intercalated anions located in the interlayer gallery for charge balance.[33,34] The intercalated anions are exchangeable, thus making it possible to adjust the interlayer spacing. Recently, our group reported a novel strategy of fabricating an ordered layered composite of two kinds of one-atom-thick sheets, graphene oxide (GO) and Co–Al layered double-hydroxide nanosheets (Co-Al LDH-NS), through electrostatic interaction as electrode materials for pseudocapacitors.[35,36] The layered composite was loosely packed, with an interlayer distance between GO and Co-Al LDH-NS of about 1 nm. The electrochemical measurements showed that the composite exhibited promising pseudocapacitive performance due to its ordered and relatively loose structure. In this work, we investigate systematically the effect of accessible space to electrolyte ions on the electrochemical activity in the system of transition metal hydroxide-based pseudocapacitors. Through an anion exchange reaction, three types of α-$Co(OH)_2$ (dodecyl sulfate-, benzoate-, and nitrate-intercalated) nanocones with interlayer distances of 1.6, 0.7, and 0.09 nm, respectively, are fabricated. The results of electrochemical measurements show that α-$Co(OH)_2$ with interlayer spacing of 1.6 nm behaves more adequately in terms of Faradaic reaction than do the others. The electrochemical activity obviously reduces when the interlayer space is 0.7 nm. This is the first report of studying the lower size limit of accessible hollow spaces in transition metal hydroxide-based ECs. Our results suggest the importance of rational design of the interlayer space of layered transition metal hydroxides for achieving high capacitance and provide a theoretical guidance for designing high-performance ECs.

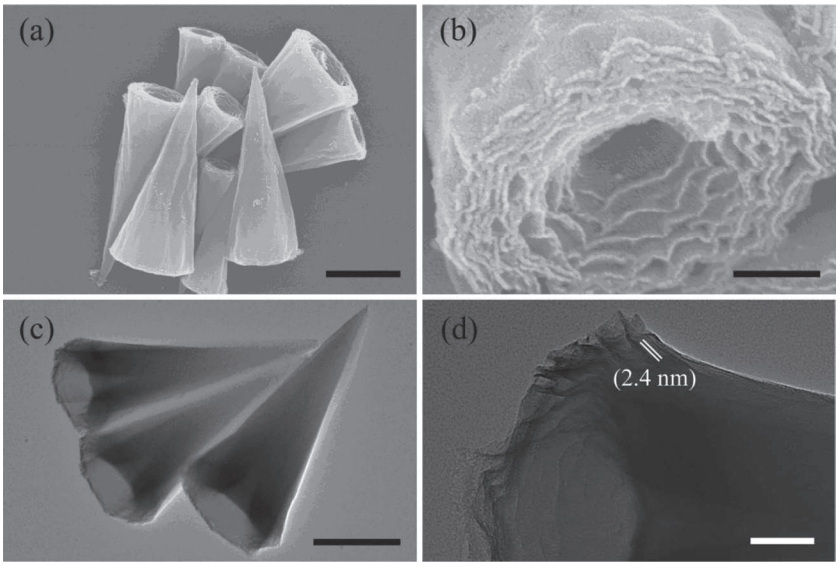

Figure 1. a) SEM and b) enlarged SEM images of DS-α-$Co(OH)_2$ (scale bars represent 1 μm in (a) and 200 nm in (b). c) TEM (scale bar is 1 μm), and, d) HR-TEM (scale bar represents 50 nm) images of DS-α-$Co(OH)_2$.

2. Results and Discussion

2.1. Structural Characterization of Various α-$Co(OH)_2$ Nanocones

Figure 1 shows the structure and morphology characterization of DS-α-$Co(OH)_2$. A large amount of nanocones with uniform structure and smooth surface are observed (Figure 1a). The nanocones have an average bottom diameter of approximate 1 μm and the length of around 3 μm. Figure 1b clearly demonstrates that the nanocone possesses multilayered structure with hollow interior (Figure 1c). The formation of DS-α-$Co(OH)_2$ nanocones is assumed to undergo similar process as described in the work of Liu et al.[37] Dodecyl sulfate-intercalated lamellar structures with few layers are firstly formed and then curl up at the edge, which produces a conical angle rather than a tubular structure owing to their morphological features and lower energy barrier. Figure 1d is a high-resolution transmission electron microscopy (HR-TEM) image which shows an ordered multilayered structure with interlayer spacing of 2.4 nm. Previous results have confirmed that the thickness of a single layer of layered double hydroxide (LDH) nanosheets is ca. 0.8 nm.[38] Therefore, the distance between adjacent layers is calculated to be 1.6 nm. Taken the molecular length of dodecyl sulfate (calculated to ca. 1.9 nm) into consideration, it is inferred that the dodecyl sulfate ions arrange perpendicularly to cobalt hydroxide nanosheet but with a tilt angle of ca. 25°.

The layered structure of DS-α-$Co(OH)_2$, benzoate-α-$Co(OH)_2$, and NO_3^--α-$Co(OH)_2$ was also confirmed by X-ray diffraction (XRD) analysis, as shown in **Figure 2**a. A basal reflection series corresponding to 2.4 nm can be clearly discerned in the case of DS-α-$Co(OH)_2$, which is consistent with the result of TEM observations. As for NO_3^--α-$Co(OH)_2$ and benzoate-α-$Co(OH)_2$, their interlayer spaces are 0.09 and 0.7 nm, respectively. Fourier transform infrared (FT-IR) spectra were used to confirm the existence of interlayer anions, as shown in Figure 2b. In the spectrum of DS-α-$Co(OH)_2$, the bands at 2924 and 2854 cm^{-1} are ascribed to the asymmetric and symmetric CH_2 stretching vibrations of alkyl chains of dodecyl sulfate, respectively, while the relatively weak band at 2954 cm^{-1} is due to the stretching vibration of the terminal CH_3 group of the hydrocarbon tail. In addition, the series of bands in the range 1300 to 900 cm^{-1} coming from the stretching mode of sulfate (OSO_3^-) are clearly seen in the spectrum. In the spectra of NO_3^--α-$Co(OH)_2$ and benzoate-α-$Co(OH)_2$, the characteristic bands attributed to dodecyl sulfate are no longer recognized. Instead, an intense absorption band at 1384 cm^{-1} due to N–O stretching vibration of NO_3^- in the case of NO_3^--α-$Co(OH)_2$ and the series of absorbance bands in the range of 1650 to 1300 cm^{-1} due to the

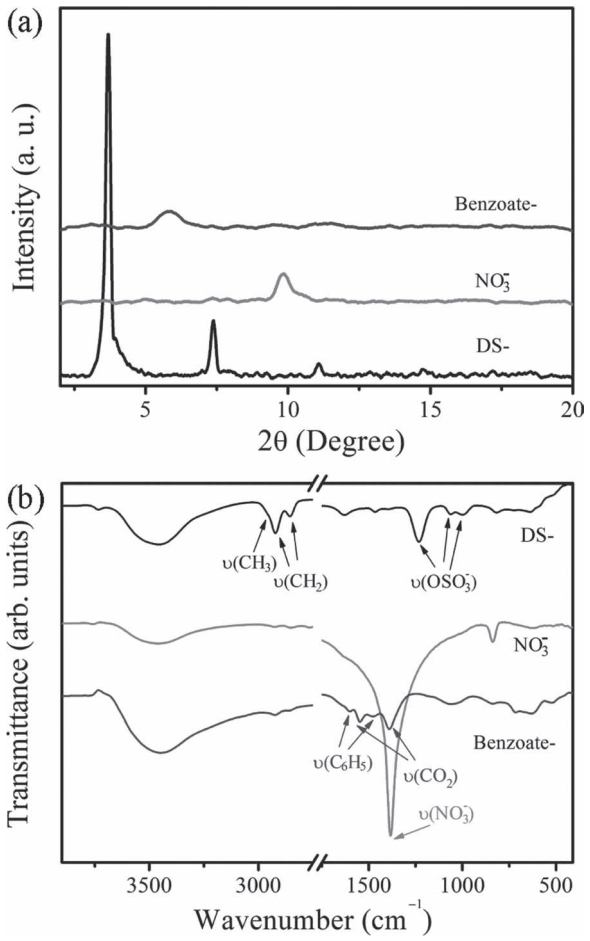

Figure 2. a) XRD patterns, and, b) FT-IR spectra of DS-α-$Co(OH)_2$, benzoate-α-$Co(OH)_2$, and NO_3^--α-$Co(OH)_2$.

stretching mode of benzyl (at 1608 and 1477 cm^{-1}) and carbonyl (at 1546 and 1392 cm^{-1}) in the case of benzoate-α-$Co(OH)_2$ are observed. These results indicate that α-$Co(OH)_2$ nanocones are highly anion-exchangeable and dodecyl sulfate are successfully exchanged by NO_3^- and benzoate. It is noteworthy that the preparation of layered α-$Co(OH)_2$ nanocones with high quality in our work is through simply refluxing hexamethylenetetramine (HMT), which is different from previous reported methods relying on either microwave-assisted or hydrothermal methods. The simplicity of refluxing makes the operation easy to achieve and readily scalable.

The structure and morphology of NO_3^--α-$Co(OH)_2$ and benzoate-α-$Co(OH)_2$ were also characterized by scanning electron microscopy (SEM) and TEM. As shown in **Figure 3**, conical structures are still obtained in both the two cases. However, a pronounced decrease of outer and inner diameters of nanocones is observed compared to the case of DS-α-$Co(OH)_2$. The surface of each nanocone appears to shrink after exchanged with NO_3^- and benzoate.

2.2. Electrochemical Activity of Various α-$Co(OH)_2$ Nanocones

First, cyclic voltammetry (CV) was used to test the electrochemical activity of the three types of α-$Co(OH)_2$. As

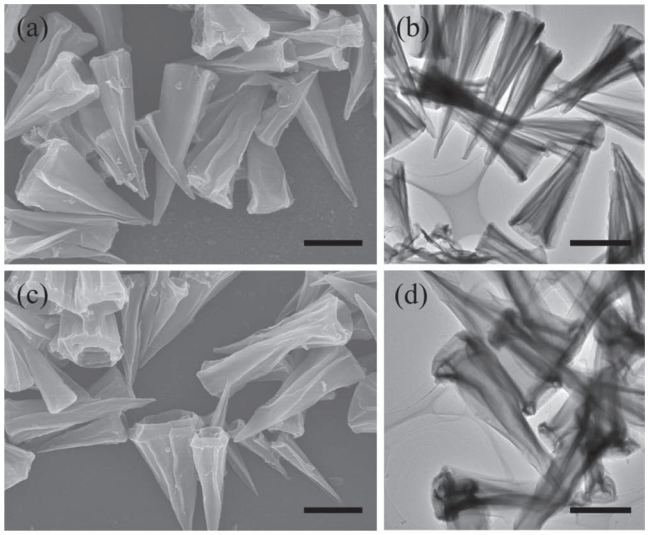

Figure 3. a) SEM, and, b) TEM images of NO_3^--α-$Co(OH)_2$. c) SEM, and, d) TEM images of benzoate-α-$Co(OH)_2$. All of the scale bars represent 1 μm.

shown in **Figure 4**, current peaks which correspond to redox Faradaic reaction could be seen in all the curves, indicating the peusdocapacitance characteristic of transition metal oxide- or hydroxide-based electrode materials. This is distinct from that of the electric double-layer capacitance, which usually produces a CV curve close to a smooth rectangular shape. In case of DS-α-$Co(OH)_2$, two quasi-reversible electron-transfer processes are visible at 0.075, –0.03 V and 0.32, 0.22 V. The potential differences in the two pairs of anodic peak and cathodic peak are both higher than 0.1 V. Theoretically, for a reversible, single-electron-transfer redox process in solution, the potential difference in a pair of anodic peak and cathodic peak is expected to be 0.058 V. Two plausible reactions are:[39]

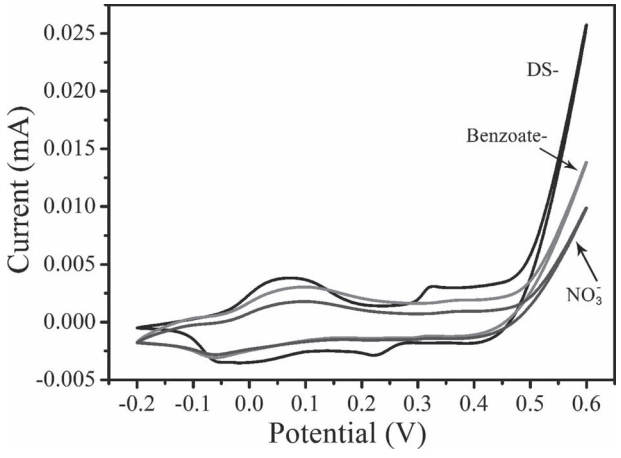

Figure 4. CV curves of DS-α-$Co(OH)_2$, NO_3^--α-$Co(OH)_2$ and benzoate-α-$Co(OH)_2$ at a sweep rate of 1 mV s^{-1} with a potential window of –0.2 to 0.6 V vs standard calomel electrode (SCE).

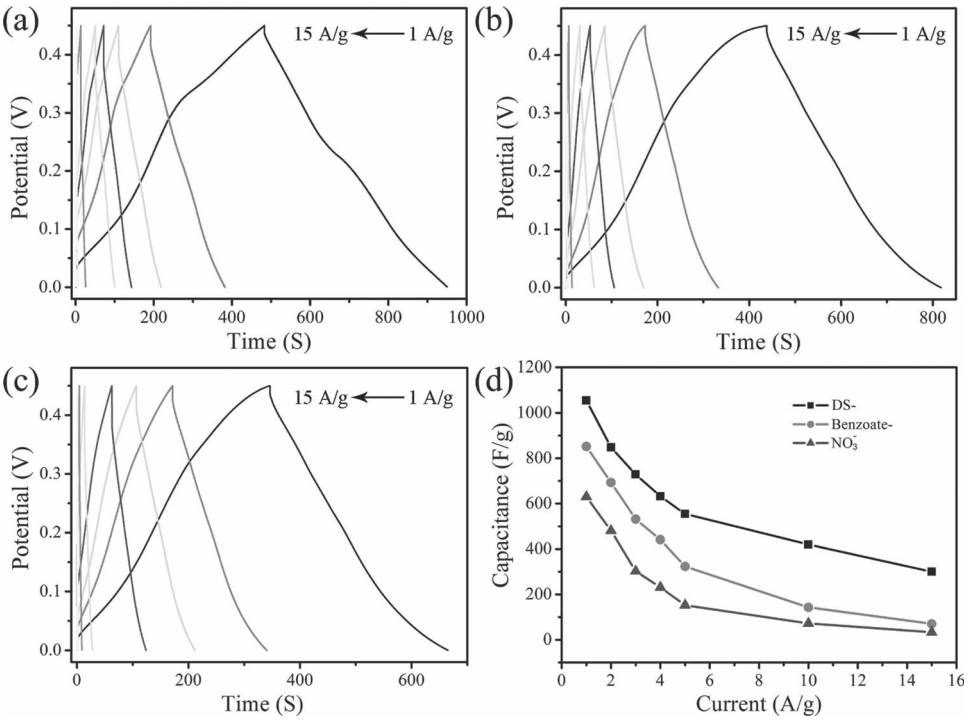

Figure 5. Galvanostatic charge/discharge curves of: a) DS-α-$Co(OH)_2$, b) NO_3^--α-$Co(OH)_2$, and, c) benzoate-α-$Co(OH)_2$ at various current densities. d) Capacitance vs current density curves of DS-α-$Co(OH)_2$, NO_3^--α-$Co(OH)_2$, and benzoate-α-$Co(OH)_2$.

$$Co(OH)_2 + OH^- \longleftrightarrow CoOOH + H_2O + e^- \quad (1)$$

$$Co(OH)_2 + OH^- \longleftrightarrow CoO_2 + H_2O + e^- \quad (2)$$

In the CV curves of NO_3^--α-$Co(OH)_2$ and benzoate-α-$Co(OH)_2$, only one redox peak, corresponding to Equation (1), is observed and the redox peak corresponding to Equation (2) is not distinguished. As intercalated anions do not contribute to electrochemical activity, they are thought to have no contribution to electrochemical response. Therefore, this indicates that the interlayer distance between adjacent $Co(OH)_2$ single sheets has a great effect on electrochemical activity of α-$Co(OH)_2$ nanocones. It is acknowledged that Faradaic reaction only occurs on the interface between electrolyte and active electrode materials. Therefore, a suitable space to allow the electrolyte to soak is required. Our results clarify that Faradaic reaction in DS-α-$Co(OH)_2$ is adequate owing to large interlayer distance up to 1.6 nm. When the interlayer distance decreases to 0.7 nm, in the case of benzoate-α-$Co(OH)_2$, the Faradaic reaction could not proceed sufficiently as the narrowed space between two $Co(OH)_2$ single sheets may hinder the fully soaking of electrolyte. The situation in case of NO_3^--α-$Co(OH)_2$ becomes worse where the interlayer distance is only 0.09 nm: the redox peak corresponding to Equation (1) is weakened compared to that of benzoate-α-$Co(OH)_2$. Therefore, the interlayer space between adjacent $Co(OH)_2$ single sheets serves as "ion-buffering reservoirs" of electrolyte ions during electrochemical processes, which ensures that sufficient Faradaic reaction can take place.

2.3. Capacitive Performance of Various α-$Co(OH)_2$ Nanocones

Figure 5a–c present the galvanostatic charge–discharge plots of DS-α-$Co(OH)_2$, NO_3^--α-$Co(OH)_2$, and benzoate-α-$Co(OH)_2$ at different current densities. All the samples show symmetric triangular charge–discharge curves with well-defined plateaus, suggesting good supercapacitive behavior. The specific capacitance of the three samples at different current densities was calculated based on these curves, as presented in Figure 5d. DS-α-$Co(OH)_2$ exhibits the highest capacitance value. Capacitances of 1055, 848, 729, 632, 555, 420, and 300 F g^{-1} corresponding to current densities of 1, 2, 3, 4, 5, 10, and 15 A g^{-1} are obtained. Corresponding to the same set of current densities, benzoate-α-$Co(OH)_2$ exhibits capacitances of 852, 693, 532, 441, 323, 143, and 70 F g^{-1} and NO_3^--α-$Co(OH)_2$ values of 630, 481, 302, 231, 152, 72, and 33 F g^{-1}. These results also demonstrate that an adequate interlayer space is beneficial to capacitance due to sufficient Faradaic reaction, in agreement with the CV measurements. Additionally, it is noted that the decrease of the specific capacitance with increase of current density in the case of DS-α-$Co(OH)_2$ is much slower than for benzoate-α-$Co(OH)_2$ or NO_3^--α-$Co(OH)_2$. A 60.2% loss of the specific capacitance (from 1055 to 420 F g^{-1}) is found for DS-α-$Co(OH)_2$ when the current density increases from 1 to 15 A g^{-1}. Correspondingly, a sharp loss of 91.8% and 95.8% of the specific capacitance (from 852 to 70 F g^{-1} and from 630 to 33 F g^{-1}) is obtained in the case of benzoate-α-$Co(OH)_2$ and NO_3^--α-$Co(OH)_2$, respectively, when the current density increases from 1 to 15 A g^{-1}. This indicates that the broader

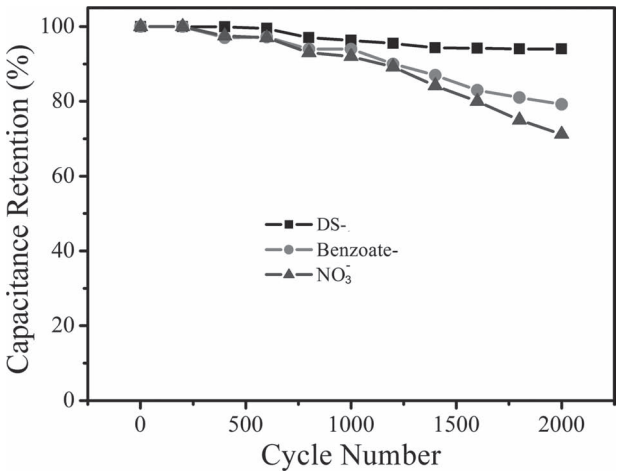

Figure 6. Capacitance retention vs cycle number curves of DS-α-$Co(OH)_2$, NO_3^--α-$Co(OH)_2$, and benzoate-α-$Co(OH)_2$ at a current density of 5 A g^{-1}.

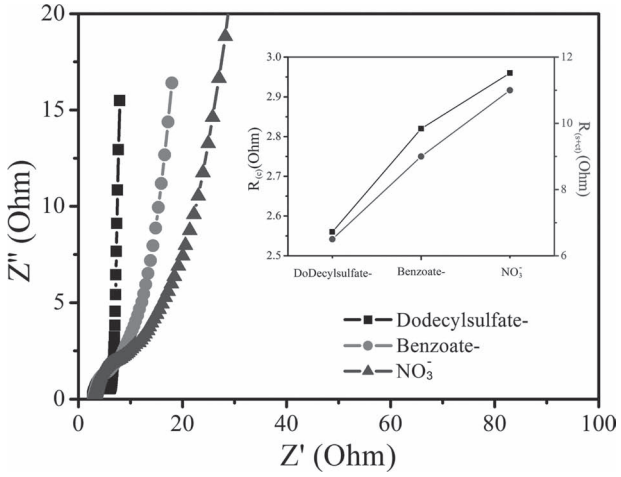

Figure 7. Electrochemical impedance spectra (EIS) of DS-α-$Co(OH)_2$, NO_3^--α-$Co(OH)_2$, and benzoate-α-$Co(OH)_2$. The inset shows R_e and $R_{(s+ct)}$.

interlayer space is helpful for fast adsorption of OH^- onto the surface of $Co(OH)_2$ passing through the interstitial space of two $Co(OH)_2$ single sheets, and thus maintaining sufficient electrochemical reaction between $Co(OH)_2$ and electrolyte ions even at higher current density and within short time. The cycling stability of DS-α-$Co(OH)_2$, NO_3^--α-$Co(OH)_2$, and benzoate-α-$Co(OH)_2$ were investigated at a charge/discharge current of 5 A g^{-1} for 2000 cycles as shown in **Figure 6**. DS-α-$Co(OH)_2$ displays good cycling stability. Nearly 95% of capacitance is retained after 2000 cycles, whereas only 81%, and 72% of capacitance is retained for NO_3^--α-$Co(OH)_2$ and benzoate-α-$Co(OH)_2$, respectively. The good cyclic performance of DS-α-$Co(OH)_2$ indicates that a broader interlayer space is better for cycling stability, which is probably due to sufficient electrolyte being supplied for redox reaction in the broader interlayer space during electrochemical processes.

2.4. Electrochemical Impedance Measurements and Schematic Drawings of Various α-$Co(OH)_2$ Nanocones

To investigate the electrode kinetics, the apparent activation energies of α-$Co(OH)_2$ with different interlayer anions were measured from electrochemical impedance spectra (EIS). **Figure 7** shows Nyquist plots of DS-α-$Co(OH)_2$, NO_3^--α-$Co(OH)_2$, and benzoate-α-$Co(OH)_2$. The values of ohmic resistance of the electrolyte and cell components (R_e) are 2.56, 2.82, and 2.96 Ω for DS-α-$Co(OH)_2$, NO_3^--α-$Co(OH)_2$, and benzoate-α-$Co(OH)_2$, respectively. These results show that the electrodes have been properly fabricated and could be tested in the same condition. Due to the single semicircle observed, the impedance can be ascribed to the combination of surface and charge-transfer resistance $R_{(s+ct)}$. The value of $R_{(s+ct)}$ is much smaller for the DS-α-$Co(OH)_2$-based electrode (6.5 Ω) than that of benzoate-α-$Co(OH)_2$ (9.0 Ω) and NO_3^--α-$Co(OH)_2$ (11.2 Ω), which means that the DS-α-$Co(OH)_2$ has a faster charge-transfer process than the others. It can be seen that the low-frequency tail for the three samples is also different. The DS-α-$Co(OH)_2$-based electrode shows a nearly vertical line, indicating a higher electron mobility, owing to the broader interlayer space.

A schematic illustration was drawn to explain the space effect on electrochemical activity of layered α-$Co(OH)_2$ (**Figure 8**). There are two types of coordination between Co (II) and hydroxyl ions: octahedral Co (II) and tetrahedral Co (II). A pair of tetrahedral Co (II) sites is generated both above and below one octahedral vacancy, sharing three hydroxyl ions with other neighboring octahedra. The tetrahedral fourth apex pointing into the interlayer space is occupied by anion ions. The thickness of $Co(OH)_2$ single sheet is about 0.8 nm and the interlayer distances for DS-α-$Co(OH)_2$, NO_3^--α-Co(OH), and benzoate-α-$Co(OH)_2$ are 1.6, 0.09, and 0.7 nm, respectively, as obtained from the above measurements. The interlayer space could be considered as an electrolyte-buffering reservoir: the larger the interlayer space, the more electrolyte ions can be stored. As discussed above, pseudocapacitance originates from a fast and reversible Faradaic reaction between electrolyte and active electrode material. To accomplish this process, two aspects must be examined: one is the large quantity of electrochemical active sites for Faradaic reaction; the other is sufficient electrolyte ions and electrons simultaneously participating in Faradaic reaction at high rates. Unlike carbon-based EDLCs, transition metal hydroxide-based pseudocapacitors have poor conductivity. Therefore, good contact between electrolyte and active electrode materials – which means sufficient soaking of electrolyte onto the surface of active electrode materials – is essential to assure high electrochemical activity, that is to say, high capacitance.

3. Conclusions

In summary, three types of layered α-$Co(OH)_2$ nanocones with different intercalated anion ions (dodecyl sulfate, nitrate, and benzoate) were fabricated by a hydrolysis of hexamethylenetetramine (HMT) through reflux and a subsequent anion-exchange process. Different to previously reported microwave-assisted or hydrothermal processes, our method

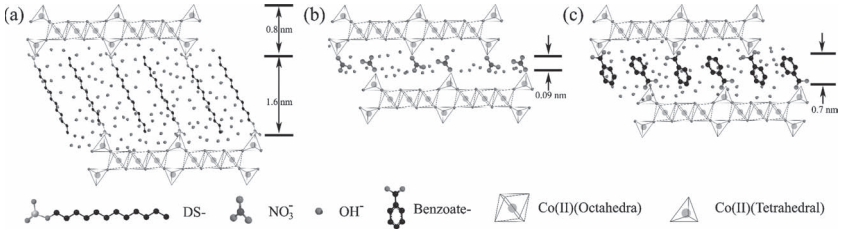

Figure 8. Schematic drawings of: a) DS-α-$Co(OH)_2$, b) NO_3^--α-Co(OH), and, c) benzoate-α-$Co(OH)_2$, where electrolyte ions (OH^-) soak into the interlayer of two adjacent single sheets of $Co(OH)_2$.

is easily performed and could be extended to further prepare layered transition metal hydroxides with various intercalated anions.[37,38] Due to the different size of intercalated anions, the three-layered α-$Co(OH)_2$ nanocones exhibited different interlayer spacing, which provides us an ideal model to investigate the space-effect on electrochemical activities as electrode materials for the use of pseudocapacitors. Our results show that the interlayer space and electrochemical activity are closely related. DS-α-$Co(OH)_2$, with an interlayer distance of 1.6 nm, displayed the highest electrochemical activity and capacitance, which had smaller interlayer distances. This indicates that larger interlayer spacing, allowing more electrolyte ions to be stored, leads to a higher electrochemical activity. The study of electrochemical activity in a tuned space helps us to deeply understand the mechanism of ionic transport in layered electrode materials. Our findings should allow the rational design of high-performance peusdocapacitors. With an in-depth understanding of the relationship between morphology and electrochemical activity, it is believed that breakthroughs in this area will spark the development of promising ECs with good performance in the near future.

4. Experimental Section

Synthesis of Dodecyl Sulfate-Intercalated α-Phase Cobalt Hydroxide Nanocones (DS-α-$Co(OH)_2$): In a three-necked flask filled with N_2 gas, $CoCl_2 \cdot 6H_2O$, sodium dodecyl sulfate (SDS), and hexamethylenetetramine (HMT) were dissolved in 1000 cm^3 of deionized water to final concentrations of 5, 20, and 15 mM, respectively. The reaction solution was then heated to 95 °C with magnetic stirring. After 5 h, a suspension containing green particles was produced. The product was filtered and washed with deionized water and anhydrous ethanol several times, and finally air-dried at room temperature.

Synthesis of Benzoate-Intercalated α-Phase Cobalt Hydroxide Nanocones (Benzoate-α-$Co(OH)_2$) and Nitrate-Intercalated α-phase Cobalt Hydroxide Nanocones (NO_3^--α-$Co(OH)_2$): the benzoate-α-$Co(OH)_2$ and NO_3^--α-$Co(OH)_2$ were prepared by an anion-exchange reaction of DS-α-$Co(OH)_2$. Typically, 0.5 g DS-α-$Co(OH)_2$ was dispersed into 500 mL of ethanol–water binary solution (1:1 v/v) containing either 0.5 M sodium benzoate or 1 M sodium nitrate in a flask. The flask was tightly capped and mechanically shaken for 24 h at room temperature after purging with N_2 gas. The product was filtered and washed with deionized water and anhydrous ethanol several times, and finally air-dried at room temperature.

Structural Characterization: X-ray diffraction (XRD) data were recorded on a Bruker D8 diffractometer with a monochromatic Cu Kα radiation (λ = 1.54 Å). The morphologies and dimensions of the as-prepared products were examined with a Hitachi S4800 field emission scanning electron microscope (FE-SEM). Transmission electron microscopy (TEM) and high-resolution transmission electron microscopy (HRTEM) were performed using a JEOL JEM-3000F transmission microscope.

Electrochemical Characterization: Electrochemical measurements were carried out in a 2 M aqueous KOH in a half-cell setup configuration at room temperature. Platinum wire and a standard calomel electrode (SCE) served as counter and reference electrodes, respectively. The working electrode was prepared by casting a slurry containing α-$Co(OH)_2$ nanocones, carbon black, and poly(vinylidene fluoride) (PVDF) in a weight ratio of 80:10:10 onto a 1 cm × 1 cm Ni foam (2 mm thick, 100 ppi, 95% porosity, purchased from Bitaxiang Co. Ltd., Kunshan, China). The electrodes were calendared and degassed in vacuum at 80 °C for at least 12 h. The resulting electrode was pressed at 5 MPa for electrochemical tests. The mass of α-$Co(OH)_2$ nanocones was accurately determined using a microbalance with 0.001 mg resolution (Sartarious). The mass loading of slurry on working electrode is 1 to 2 mg in each. Cyclic voltammetry (CV), chronopotentiometry, and electrochemical impedance spectra (EIS) were obtained on a CHI 660D electrochemistry workstation. CV curves were recorded at a sweep rate of 1 mV s^{-1} with a potential window of –0.2 to 0.6 V vs SCE and cycling performance was investigated at a current density of 5 A g^{-1}. EIS was collected by applying a perturbation voltage of 5 mV in a frequency range of 100 KHz to 10 mHz.

Acknowledgements

L.W. and Z.H.D. contributed equally to this work. We are grateful to Dr. Ren Zhi Ma of the National Institute for Materials Science, Japan for helpful discussions. This work was supported by the National Natural Science Foundation of China (grant no. 50973080 and 21004076) and the National Basic Research Program of China (grant no. 2010CB934700).

Received: September 25, 2012
Published online: December 17, 2012

[1] Z. G. Yang, J. L. Zhang, M. W. Kintner-Meyer, X. C. Lu, J. L. Choi, J. Liu, *Chem. Rev.* **2011**, *111*, 3577.
[2] P. Simon, Y. Gogotsi, *Nat. Mater.* **2008**, *7*, 845.
[3] M. B. Sassin, C. N. Chervin, D. R. Rolison, J. W. Long, *Acc. Chem. Res.* **2012**, DOI:10.1021/ar2002717.
[4] K. Naoi, W. Naoi, S. Aoyagi, J. I. Miyamoto, T. Kamino, *Acc. Chem. Res.* **2012**, DOI:10.1021/ar200308h.
[5] S. B. Lee, R. Liu, *J. Am. Chem. Soc.* **2008**, *130*, 2942.
[6] Z. S. Wu, W. C. Ren, D. W. Wang, F. Li, F. Liu, B. L. Liu, H. M. Cheng, *ACS Nano* **2010**, *4*, 5835.
[7] J. Y. Zhu, J. H. He, *ACS Appl. Mater. Interfaces* **2012**, *4*, 1770.
[8] K. Kai, Y. Kobayashi, Y. Yamada, K. Miyazaki, T. Abe, Y. Uchimoto, H. Kageyama, *J. Mater. Chem.* **2012**, *22*, 14691.
[9] Q. Li, Z. L. Wang, G. R. Li, R. Guo, L. X. Ding, Y. X. Tong, *Nano Lett.* **2012**, *12*, 3803.
[10] L. Y. Yuan, X. H. Lu, X. Xiao, T. Zhai, J. J. Dai, F. C. Zhang, B. Hu, X. Wang, L. Gong, J. Chen, C. Hu, Y. Tong, J. Zhou, Z. L. Wang, *ACS Nano* **2012**, *6*, 656.
[11] P. Justin, S. K. Meher, G. R. Rao, *J. Phys. Chem. C* **2010**, *114*, 5203.
[12] J. H. Kim, K. Zhu, Y. F. Yan, C. L. Perkins, A. J. Frank, *Nano Lett.* **2010**, *10*, 4099.
[13] D. W. Wang, Q. H. Wang, T. M. Wang, *Inorg. Chem.* **2011**, *50*, 6482.
[14] S. K. Meher, G. R. Rao, *J. Phys. Chem. C* **2011**, *115*, 15646.
[15] S. K. Meher, G. R. Rao, *J. Phys. Chem. C* **2011**, *115*, 25543.
[16] H. T. Wang, L. Zhang, X. H. Tan, C. M. B. Holt, B. Zahiri, B. C. Olsen, D. Mitlin, *J. Phys. Chem. C* **2011**, *115*, 17599.

[17] C. Z. Yuan, L. Yang, L. R. Hou, L. F. Shen, X. G. Zhang, X. W. Lou, *Energy Environ. Sci.* **2012**, *5*, 7883.
[18] J. H. Zhong, A. L. Wang, G. R. Li, J. W. Wang, Y. N. Ou, Y. X. Tong, *J. Mater. Chem.* **2012**, *22*, 5656.
[19] S. Chen, J. W. Zhu, X. Wang, *J. Phys. Chem. C* **2010**, *114*, 11829.
[20] M. Q. Zhao, Q. Zhang, J. Q. Huang, F. Wei, *Adv. Funct. Mater.* **2012**, *22*, 675.
[21] S. Huang, G. N. Zhu, C. Zhang, W. W. Tjiu, Y. Y. Xia, T. X. Liu, *ACS Appl. Mater. Interfaces* **2012**, *4*, 2242.
[22] Z. Y. Lu, W. Zhu, X. D. Lei, G. R. Williams, D. O'Hare, Z. Chang, X. M. Sun, X. Duan, *Nanoscale* **2012**, *4*, 3640.
[23] Q. Wang, D. O'Hare, *Chem. Rev.* **2012**, *112*, 4124.
[24] L. P. Xu, Y. S. Ding, C. H. Chen, L. L. Zhao, C. Rimkus, R. Joesten, S. L. Suib, *Chem. Mater.* **2008**, *20*, 308.
[25] J. Yan, W. Sun, T. Wei, Q. Zhang, Z. J. Fan, F. J. Wei, *Mater. Chem.* **2012**, *22*, 11494.
[26] J. X. Li, M. Yang, J. P. Wei, Z. Zhou, *Nanoscale* **2012**, *4*, 4498.
[27] M. F. Shao, F. Y. Ning, Y. F. Zhao, J. W. Zhao, M. Wei, D. G. Evans, X. Duan, *Chem. Mater.* **2012**, *24*, 1192.
[28] H. L. Wang, H. S. Casalongue, Y. Y. Liang, H. J. Dai, *J. Am. Chem. Soc.* **2010**, *132*, 7472.
[29] G. H. Yu, L. L. Hu, M. Vosgueritchian, H. L. Wang, X. Xie, J. R. McDonough, X. Cui, Y. Cui, Z. N. Bao, *Nano Lett.* **2011**, *11*, 2905.
[30] S. K. Meher, P. Justin, G. R. Rao, *ACS Appl. Mater. Interfaces* **2011**, *3*, 2063.
[31] G. H. Yu, L. B. Hu, N. Liu, H. L. Wang, M. Vosgueritchian, Y. Yang, Y. Cui, Z. N. Bao, *Nano Lett.* **2011**, *11*, 4438.
[32] J. Chmiola, G. Yushin, Y. Gogotsi, C. Portet, P. Simon, P. L. Taberna, *Science* **2006**, *313*, 1760.
[33] Z. P. Liu, R. Z. Ma, M. Osada, K. Takada, T. Sasaki, *J. Am. Chem. Soc.* **2005**, *127*, 13869.
[34] R. Z. Ma, Z. P. Liu, K. Takada, K. Fukuda, Y. Ebina, Y. Bando, T. Sasaki, *Inorg. Chem.* **2006**, *45*, 3964.
[35] L. Wang, D. Wang, X. Y. Dong, Z. J. Zhang, X. F. Pei, X. J. Chen, B. Chen, J. Jin, *Chem. Commun.* **2011**, *47*, 3556.
[36] X. Y. Dong, L. Wang, D. Wang, C. Li, J. Jin, *Langmuir* **2012**, *28*, 293.
[37] X. H. Liu, R. Z. Ma, Y. Bando, T. Sasaki, *Angew. Chem., Int. Ed.* **2010**, *49*, 8253.
[38] X. H. Liu, R. Z. Ma, Y. Bando, T. Sasaki, *Adv. Mater.* **2012**, *24*, 2148.
[39] L. Cao, F. Xu, Y. Y. Liang, H. L. Li, *Adv. Mater.* **2004**, *16*, 1853.